Electronic Supplementary Material (ESI) for Catalysis Science & Technology.

Supporting Information for

Integration of Surface Polymerization and Self-assembly Strategies for Heterogenization of Copper-based Catalyst for Water Oxidation

*Xin Li, Mengjiao Shao, Xueling Song, Xuesong Jiang, Guisheng Li, and Lei Wang**

School of Materials and Chemistry, University of Shanghai for Science and Technology, Shanghai 200093, China

Table of contents

Experimental Methods

Synthetic Methods and Materials. The ligands, pimR, were prepared according to the literature[1]. All other reagents and solvents were purchased from commercial sources and used as received.

Physical Methods. Nuclear magnetic resonance (NMR) spectra were recorded on a Bruker Avance NEO 400 WB solid-state superconducting NMR spectrometer (Fällanden, Switzerland). ^{1}H NMR spectra were referenced to TMS using the residual portion impurities of the solvent. All chemical shifts are reported in the standard δ notation in parts per million; positive chemical shifts are a higher frequency than the reference. Reported pH values were measured on a REX E-301F pH Metera glass electrode after calibration with standard buffer solutions. Contact angle test by Chengde Dingsheng JY-82C Video Contact Angle Tester. Scanning Electron Microscopy (SEM) was performed using a JEOL JSM-IT500HR instrument. UV-vis is tested by Shimadzu-2700i. Infrared spectroscopy is detected by Perkin Elmer's SPE CTRUM 100 Fourier Transform Infrared Spectrometer. Electrochemical measurements were performed with a CH Instruments CHI-760E bipotentiostat at ambient temperature (21-24 °C) in a single compartment cell with a platinum wire counter electrode, and Ag/AgCl (3 M KCl) reference electrode[2]. Electrochemical data were calibrated with respect to the NHE by incorporating a voltage shift of 0.199 V to the recorded potential measurements. All potentials are expressed in relation to NHE, unless explicitly indicated otherwise[3].

Synthetic Procedures

General description. The ligands, 1-alkyl-2-(2-pyridyl)imidazol (pimR) were synthesized by mixing 2-(2-pyridyl)imidazole and alkyl iodides at room temperature in the presence of sodium hydroxide (**Figure S1-S3**)[4]. Then the purified ligands were mixed with equimolar amounts of copper acetate and stirred in methanol for 4 h to give rise to the final product, $[Cu(pimR)(OH_2)_2]^{2+}$ (Cu-R, **Scheme S1**).

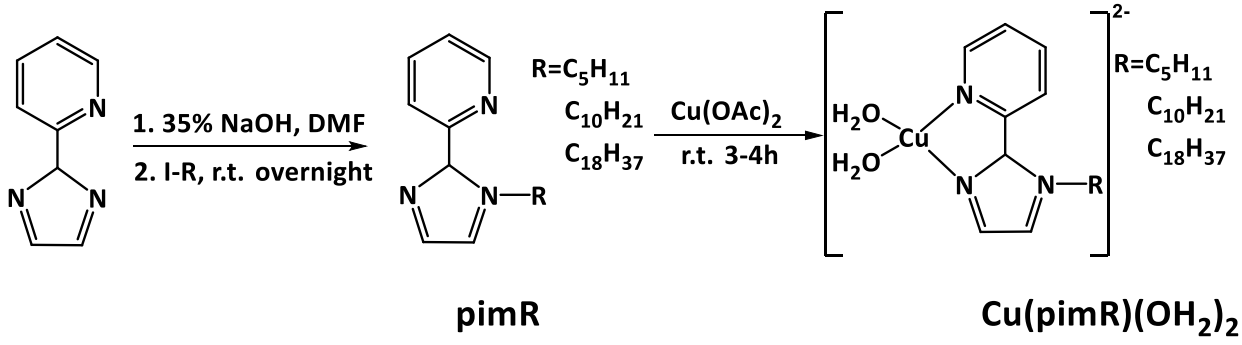

Scheme S1. Synthesis of ligand pimR and compound $Cu(pimR)(OH)_2$.

Detailed procedures. A mixture of 2-(2-pyridyl) imidazole (1 g, 6.9mmol) and 35% aqueous NaOH (1.0 mL) in DMF (10 mL) was stirred for 1 h at 25 °C Alkyl iodide (8.96 mmol) was then added slowly, and the mixture stirred overnight at 25 °C. The resulting solution was then poured into H_2O (30 ml) and extracted with chloroform (3 × 20 mL). The combined organic layers were washed with H_2O (3 × 20 mL) and dried over Na_2SO_4. After evaporating the solvent under reduced pressure, the residue was purified by flash chromatography on silica gel to give ligands pimR, where R is C_5H_{11}, $C_{10}H_{21}$, $C_{18}H_{37}$. Then the resulting ligand was mixed with $Cu(AcO)_2$ (1.3mmol, 236.12mg) and stirred for 3-4h at the room temperature with obtaining a blue solution. Removing the solvents under reduced pressure afforded the compounds $Cu(pimR)(OH_2)_2$ as the blue solid.

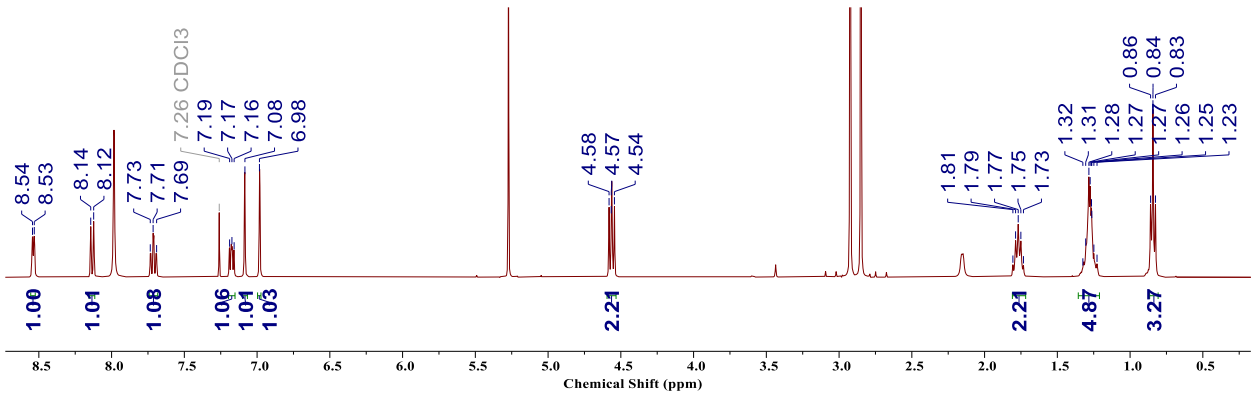

Figure S1. ^1H NMR spectrum for ligand $pimC_5H_{11}$ in $CDCl_3$. ^1H NMR (400 MHz, Chloroform-*d*) δ 8.57 (s, 1H), 8.16 (d, *J* = 8.0 Hz, 1H), 7.75 (d, *J* = 7.7 Hz, 1H), 7.23 – 7.17 (m, 1H), 7.11 (s, 1H), 7.00 (s, 1H), 4.63 – 4.54 (m, 2H), 1.78 (t, *J* = 7.3 Hz, 2H), 1.26 (d, *J* = 21.4 Hz, 14H), 0.87 (t, *J* = 6.8 Hz, 4H).

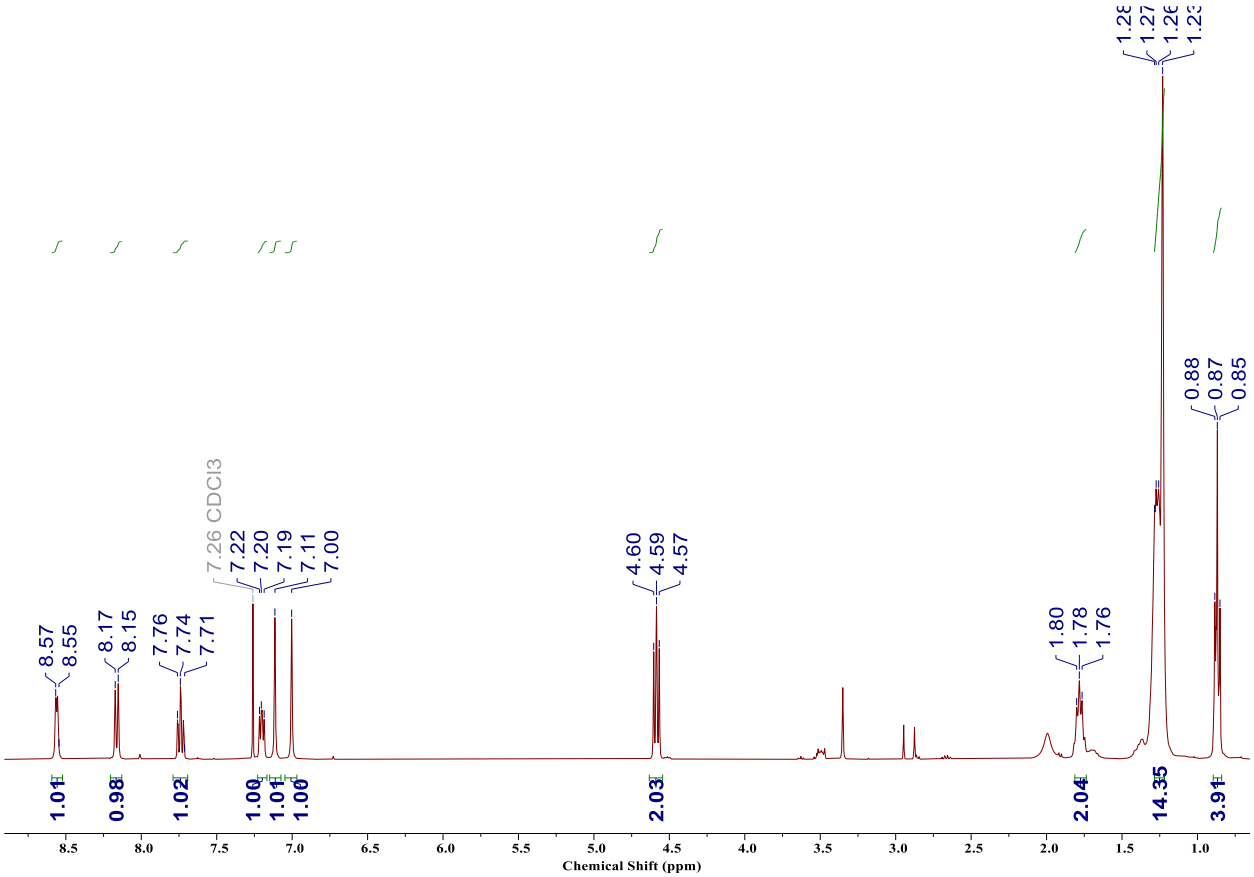

Figure S2. ^{1}H NMR spectrum for ligand pim$C_{10}H_{21}$ in $CDCl_3$. ^{1}H NMR (400 MHz, Chloroform-*d*) δ 8.54 (d, *J* = 4.9 Hz, 1H), 8.13 (d, *J* = 8.1 Hz, 1H), 7.74 – 7.68 (m, 1H), 7.20 – 7.15 (m, 1H), 7.08 (s, 1H), 6.98 (s, 1H), 4.59 – 4.53 (m, 2H), 1.77 (p, *J* = 7.3 Hz, 2H), 1.28 (hept, *J* = 6.8, 5.7 Hz, 5H), 0.84 (t, *J* = 6.8 Hz, 3H).

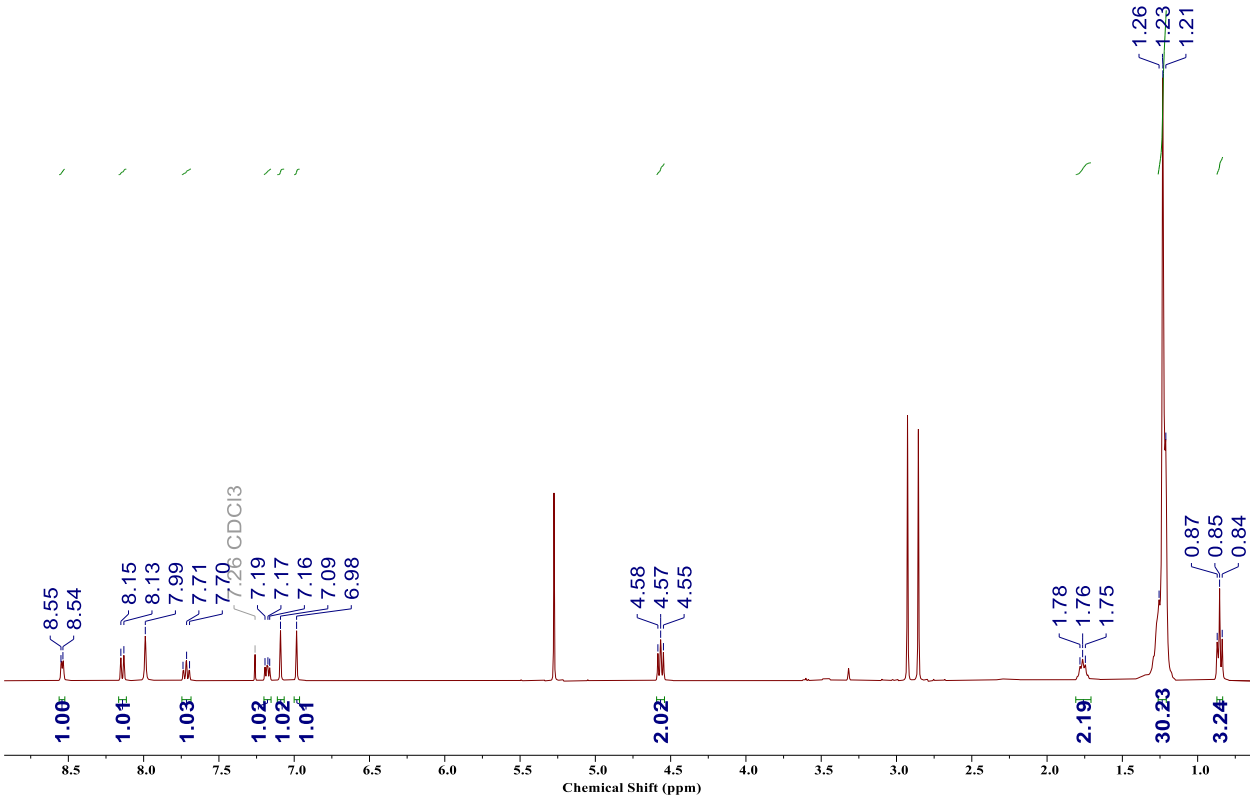

Figure S3. ^{1}H NMR spectrum for ligand pim$C_{18}H_{37}$ in $CDCl_3$. ^{1}H NMR (400 MHz, Chloroform-*d*) δ 8.54 (d, *J* = 5.2 Hz, 1H), 8.14 (d, *J* = 8.0 Hz, 1H), 7.72 (t, *J* = 8.7 Hz, 1H), 7.20 – 7.15 (m, 1H), 7.09 (s, 1H), 6.98 (s, 1H), 4.59 – 4.54 (m, 2H), 1.76 (t, *J* = 7.2 Hz, 2H), 1.22 (d, *J* = 7.9 Hz, 30H), 0.85 (t, *J* = 6.7 Hz, 3H).

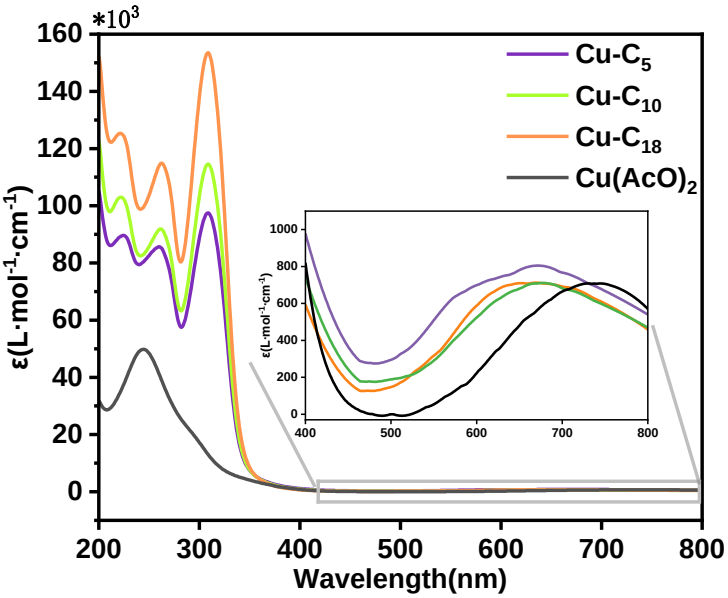

Figure S4. UV-vis spectrum of Cu-R and pristine $Cu(AcO)_2$ in methanol.

Table S1. UV-vis properties of 0.1 mM copper complexes

Cat.	medium	λ_{max} (nm)	ε (L·mol-1·cm-1)[a]
$Cu(pimH)(OH_2)_2$[5]	pH 12.2 buffer	~625	/
Cu-C_5	CH_3OH	672	804
Cu-C_{10}	CH_3OH	679	708
Cu-C_{18}	CH_3OH	679	708

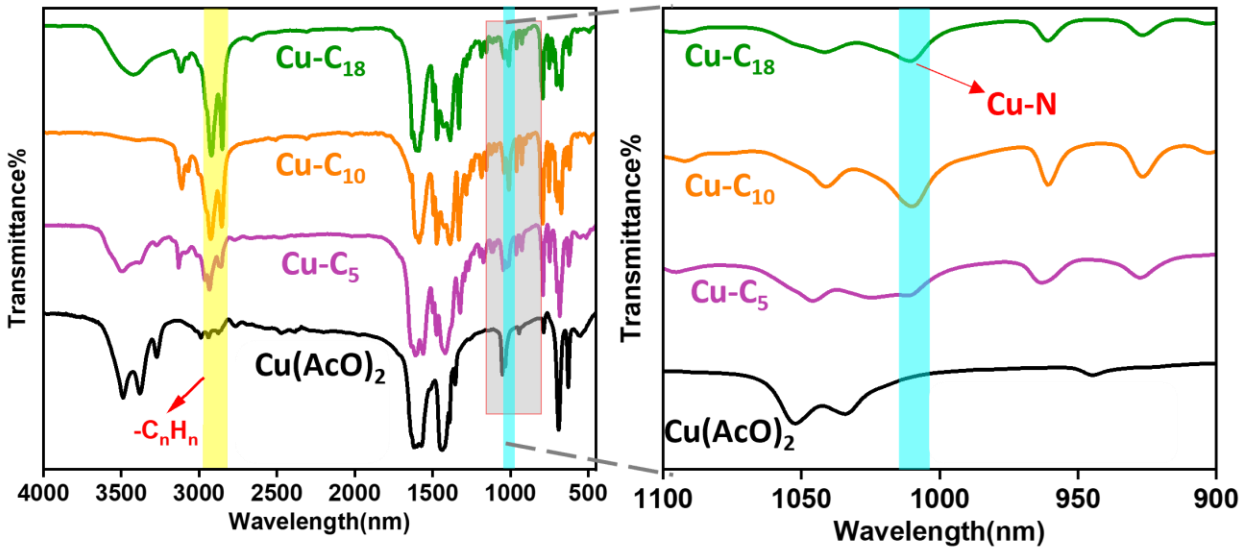

Figure S5. IR spectrum of the Cu-R catalysts powder.

Fabrication of Cu-R|SiO@FTO and PI|Cu-R|SiO@FTO

The preparation steps of Cu-R|SiO@FTO followed similar procedures as we reported previously[6]: 1) prepare 1 mM siloxane in dichloromethane (DCM) /0.1M TFA (4:1), immerse FTO slide in it for 4 h under Ar protection. 2) Rinse the above FTO slide with dichloromethane and then with hexanes and air dry to get SiO@FTO. 3) Prepare 0.2 mM catalysts in dichloromethane/ hexanes (3:1) and immerse above slide in it for 6 h. 4) Rinse FTO slide with dichloromethane and hexanes, air dry. Then **Cu-R|SiO@FTO** was obtained.

The preparation steps of PI|Cu-R|SiO@FTO are based on above steps: 1) The obtained Cu-R|SiO@FTO was immersed in 2 mL vigorous stirring mixture solution of 10 mg/mL, 35 mg/mL, or 70 mg/mL tetrakis(4-aminophenyl)methane (TAM) and 10 mg/mL 4,4'-(hexafluoroisopropylidene)diphthalic anhydride (6FDA) and stirred for 30 s. 2) 35 mL petroleum ether was poured into the mixture and stirred for 30 s, during which white suspension appears. 3) 261 µL triethanolamine and 705 µL acetic anhydride were added in above solution to terminate the reaction. 4) the obtained slide was washed with acetone for three times and air dried for 2 hours. Then **PI|Cu-R|SiO@FTO** was constructed.

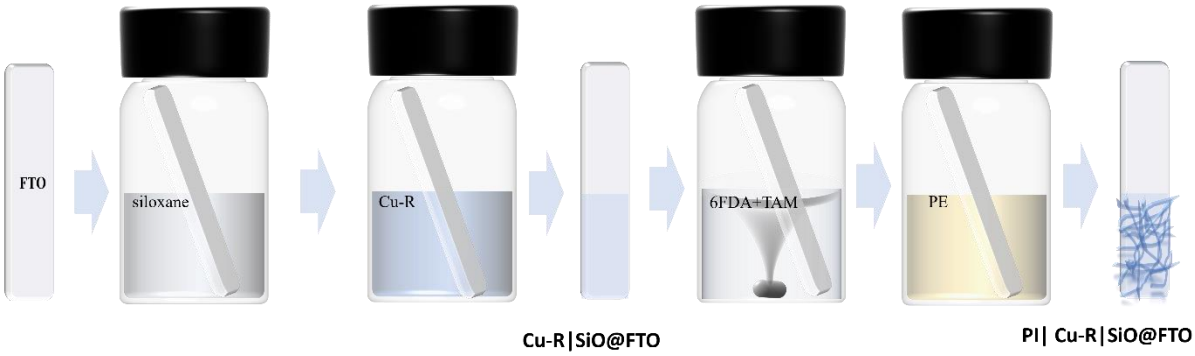

Scheme S2. Preparation steps for Cu-R|SiO@FTO and PI|Cu-R|SiO@FTO.

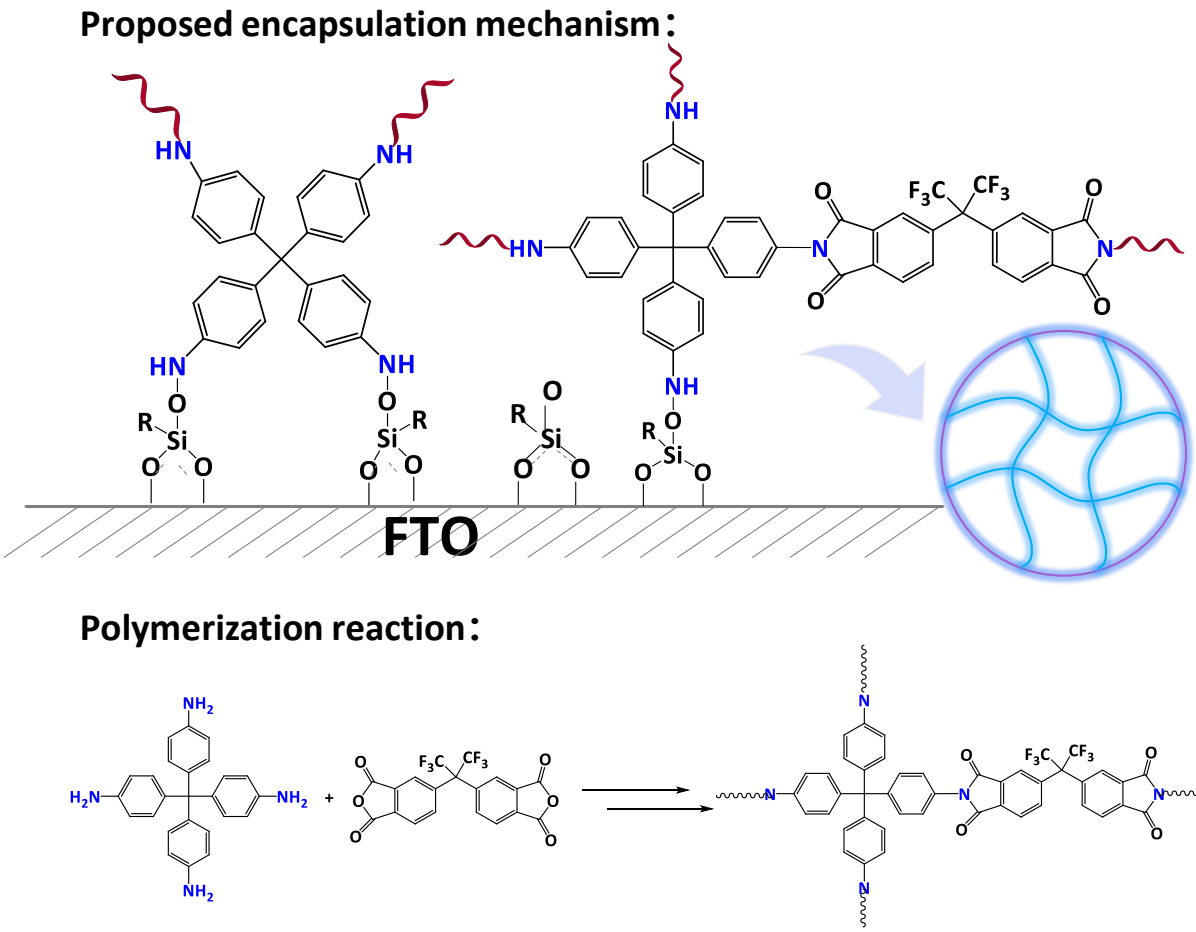

Scheme S3. Proposed encapsulation mechanisms and polymer reactions on FTO.

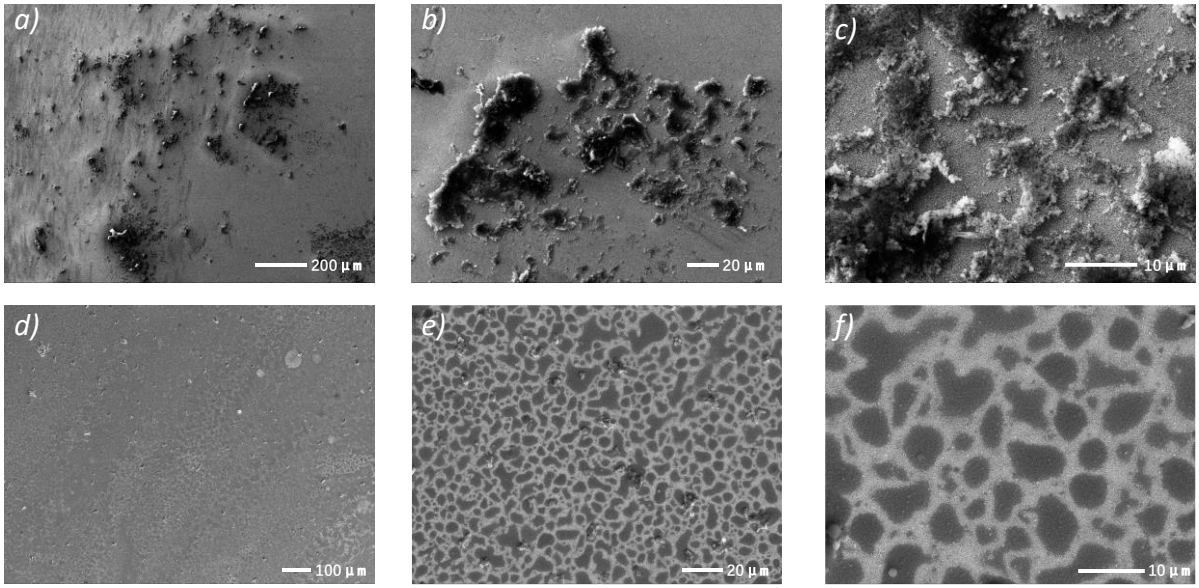

Figure S6. SEM image of PI|Cu-R|SiO@FTO by using mixture solution of a-c) TAM (70 mg/mL) and 6FDA (10 mg/mL) and d-f) TAM (35 mg/mL) and 6FDA (10 mg/mL).

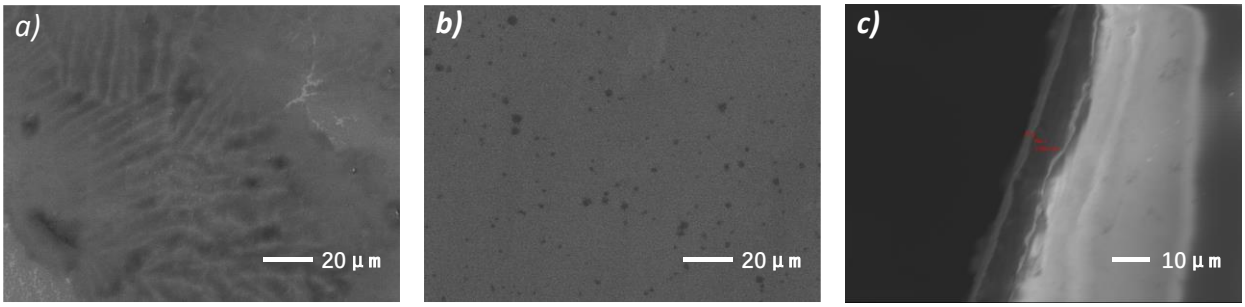

Figure S7. a-b) SEM image of Cu-R|SiO@FTO and PI|Cu-R|SiO@FTO. c) Cross-section SEM image of PI|Cu-R|SiO@FTO, displaying the thickness of the surface film.

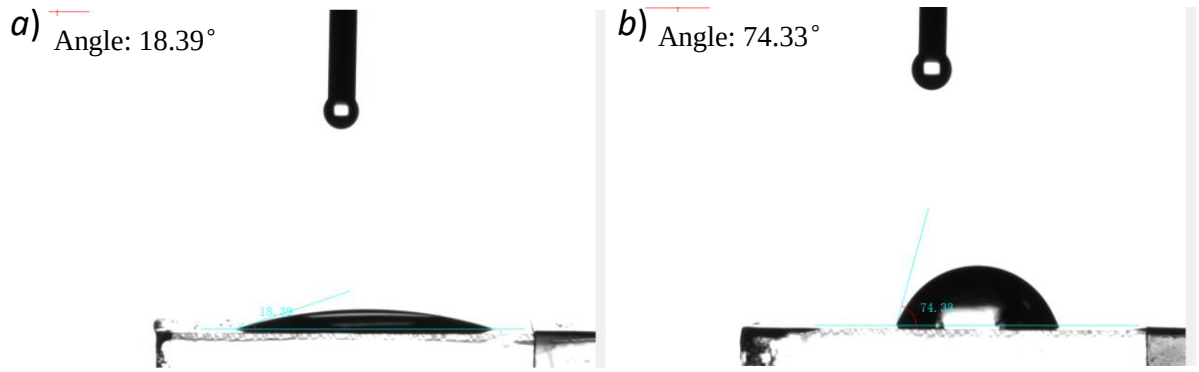

Figure S8. Contact angle measurements of a) Cu-R|SiO@FTO; b) PI|Cu-R|SiO@FTO.

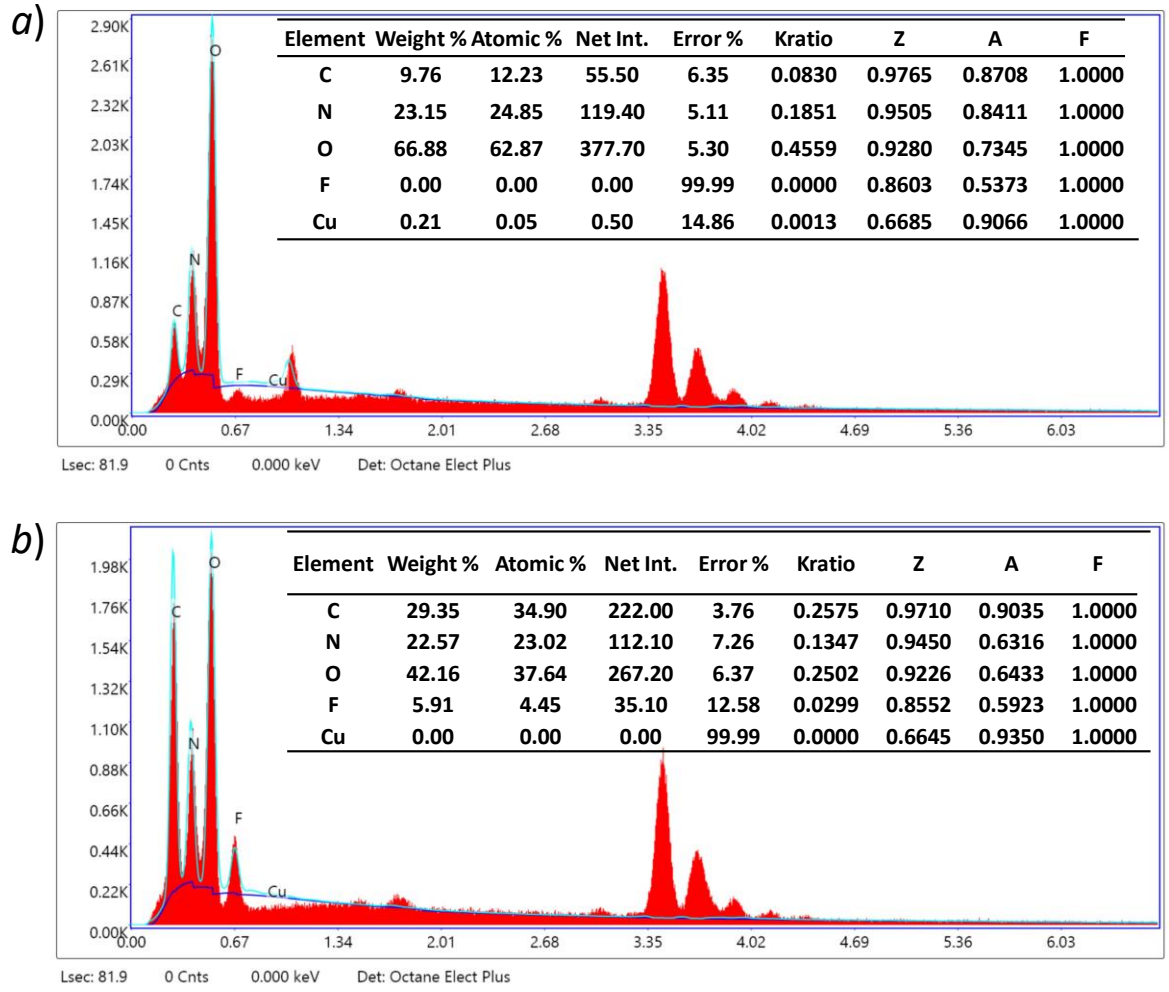

Figure S9. EDS of a) Cu-R|SiO@FTO, b) PI|Cu-R|SiO@FTO.

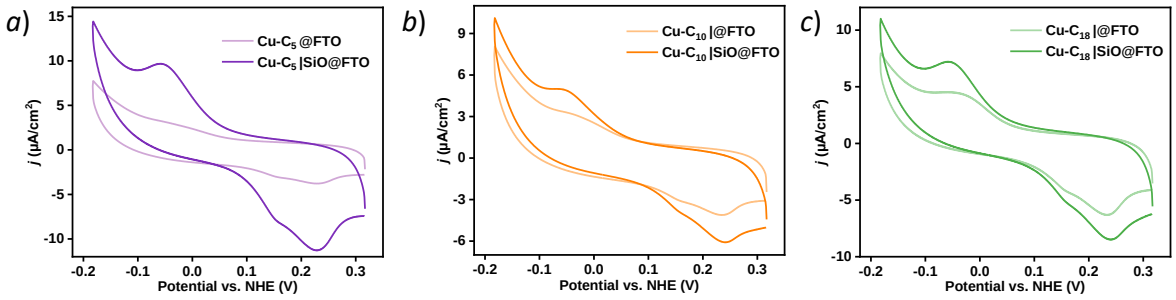

Figure S10. CVs for only Cu-R@FTO and Cu-R|Si@FTO (S = 1 cm^2, pH = 12.00, 0.1 M NaOH/NaOAc) under N_2 atmosphere.

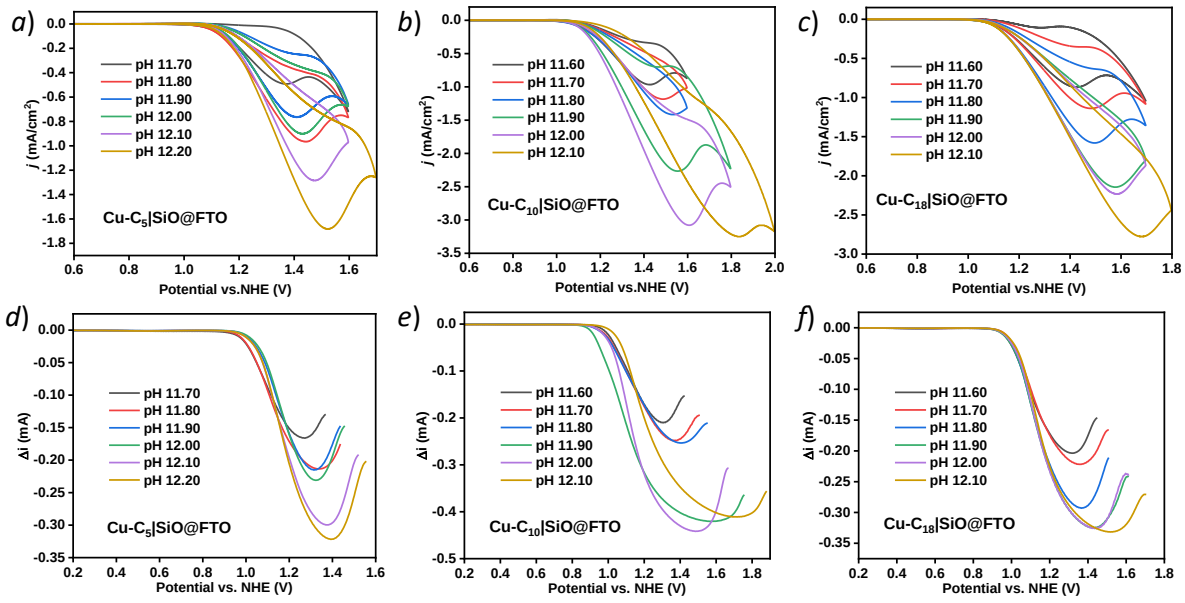

Figure S11. CVs of Cu-R|SiO@FTO under various pH for a) Cu-C_5|SiO@FTO, b) Cu-C_{10}|SiO@FTO and c) Cu-C_{18}|SiO@FTO. d-f) SWVs of corresponding Cu-R|Si@FTO under various pH buffers (S = 1 cm^2, pH 12.00, 0.1 M NaOH/NaOAc, Sweep speed:100 mV/s).

Table S2. pH-dependence of redox potentials (V vs. NHE) and peak current density (mA/cm^2) for SWVs in Figure S11.

Sample	pH	11.60	11.70	11.80	11.90	12.00	12.10	12.20
Cu-C_5|SiO@FTO	Potential (V vs NHE)	/	1.31	1.37	1.41	1.57	1.47	1.74
	Current (mA/cm^2)	/	-0.17	-0.21	-0.22	-0.23	-0.30	-0.32
Cu-C_{10}|SiO@FTO	Potential (V vs NHE)	1.31	1.37	1.41	1.57	1.47	1.74	/
	Current (mA/cm^2)	-0.21	-0.25	-0.25	-0.42	-0.43	-0.40	/
Cu-C_{18}|SiO@FTO	Potential (V vs NHE)	1.32	1.35	1.38	1.43	1.43	1.52	/
	Current (mA/cm^2)	-0.20	-0.22	-0.29	-0.30	-0.30	-0.29	/

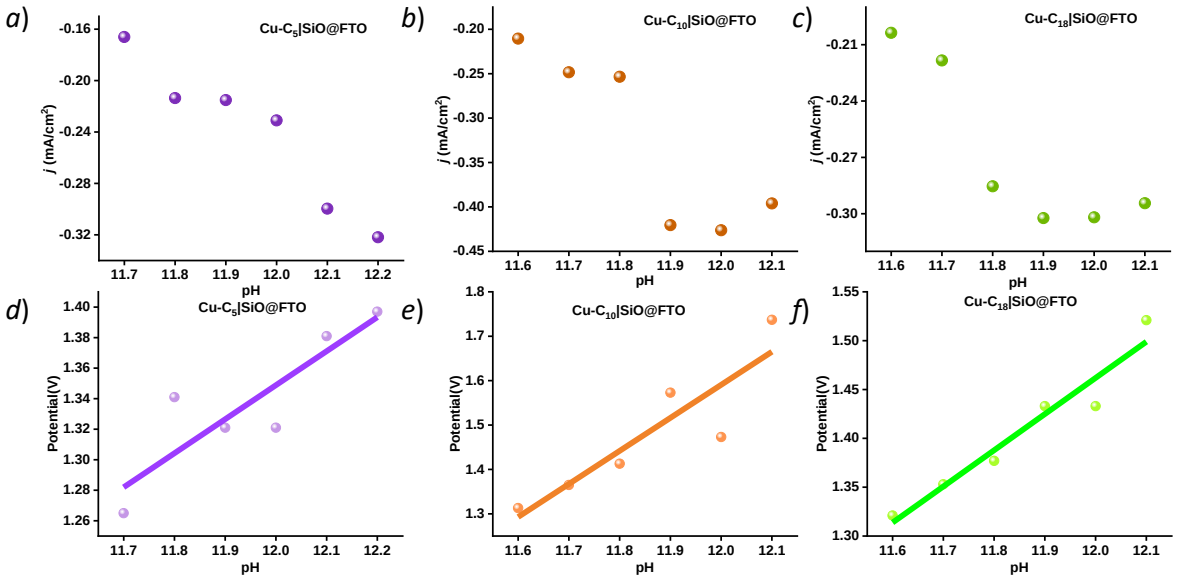

Figure S12. Variation of the water oxidation current density and potential $E_{1/2}$ (V vs. NHE) with pH. We take the peak current density and the corresponding redox potentials at each pH.

Discussion: These pH-regulated trends align with previous report[3, 5, 7]. The reason behind this is attribute to protonation and polymerization of the copper species. As the pH is increased, the pimH ligand of complex is deprotonated and is converted to $Cu(pim)(OH)_2$ monomers at high pH. These variations lead to the random changes of peak current at different pH.

Surface coverage calculations:

The surface coverage was calculated according to an established method[6]. The absorbance of the assemblies is evaluated by surface coverage, as shown in equation S1:

$$\Gamma = \frac{Q}{nFA} \qquad \text{(eq. S1)}$$

where Q is the total charge, n is the number of transferred electrons (here n = 1), A is the surface area (in our experiment, A = 1 cm^2) and F is the Faraday constant (which is 96485.3 $C \cdot mol^{-1}$).

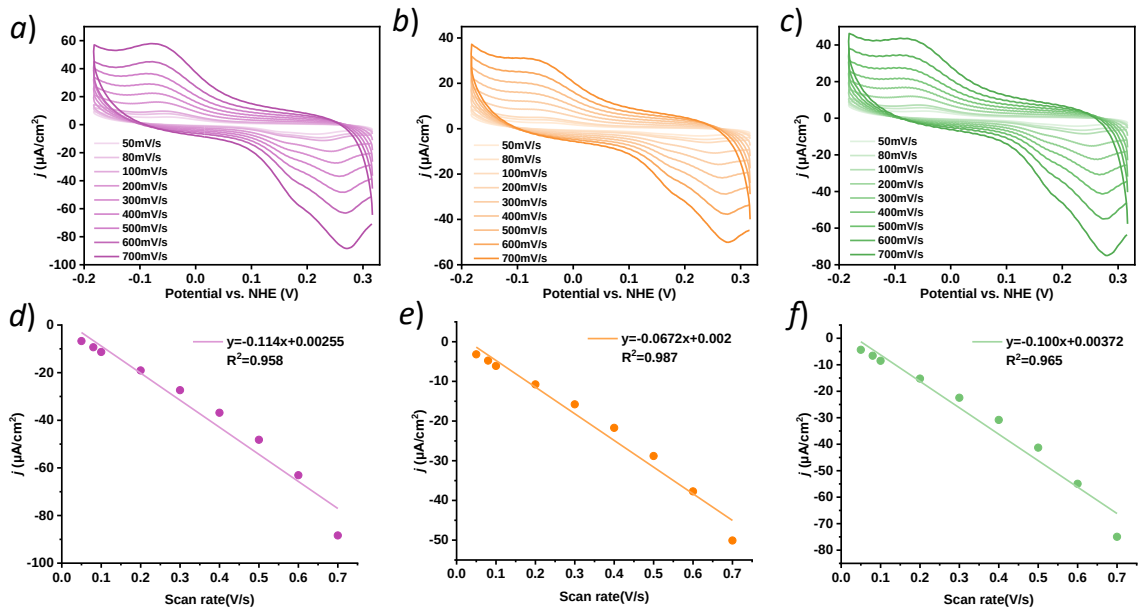

Figure S13. CVs for Cu-R|Si@FTO at different sweep scan rate and plot line of linear relationship between sweep scan and current density (S = 1 cm^2, pH = 12.00, buffer: 0.1M NaOH/NaOAc, under N_2 atmosphere). a, d) Cu-C_5|Si@FTO; b, e) Cu-C_{10}|Si@FTO; c, f) Cu-C_{18}|Si@FTO.

Discussion: We noticed that there are two oxidative peaks in the $Cu^{II/I}$ redox feature in Figure S13. This behavior has been reported for copper complexes before[5, 8, 9]. As reported by Warren et al.[5], there are many intermediates in the transition of $Cu^{II/I}$. We assumed that the two oxidative peaks are due to the existence of these intermediates.

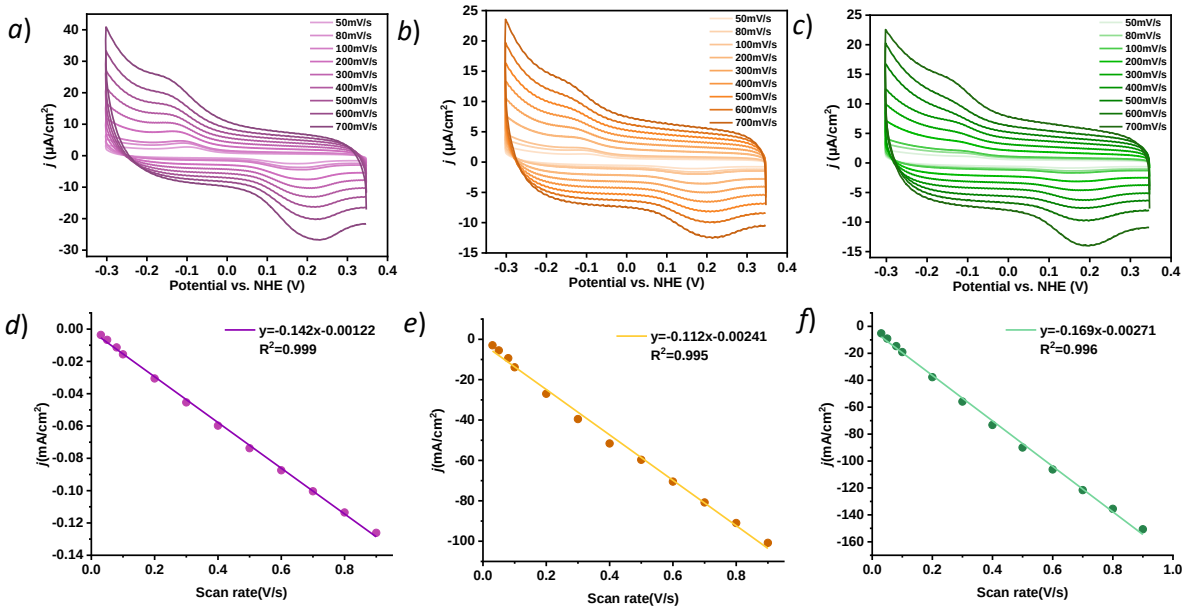

Figure S14. CVs for PI|Cu-R|Si@FTO at different sweep scan rate and plot line of linear relationship between sweep scan and current density (S = 1 cm^2, pH 12.00, 0.1M NaOH/NaOAc, under N_2 atmosphere). a, d) PI|Cu-C_5|Si@FTO; b, e) PI|Cu-C_{10}|Si@FTO; c, f) PI|Cu-C_{18}|Si@FTO.

Heterogenous electron transfer (ET) rate measurements. Transfer coefficient (α) and heterogeneous ET rate constant (k_s) was estimated from variation of peak potentials with scan rate according to Laviron's theory. When $\triangle E_p$ is larger than 0.2/n V, E_{pa}, E_{pc} shift linearly with logarithmic scan rate, yielding two straight lines. α was calculated by using slopes (k_a, k_c) of the two straight lines:

$$\log\left(\frac{k_a}{k_c}\right) = \log\left(\frac{\alpha}{1-\alpha}\right) \qquad \text{(eq. S2)}$$

The calculated α values have been summarized in **Table S1**. Then k_s was calculated by the equation eq. S3:

$$logk_s = \alpha\log(1-\alpha) + (1-\alpha)log\alpha - \log\left(\frac{RT}{nFv}\right) - \frac{\alpha(1-\alpha)\Delta E_p nF}{2.3RT} \qquad \text{(eq. S3)}$$

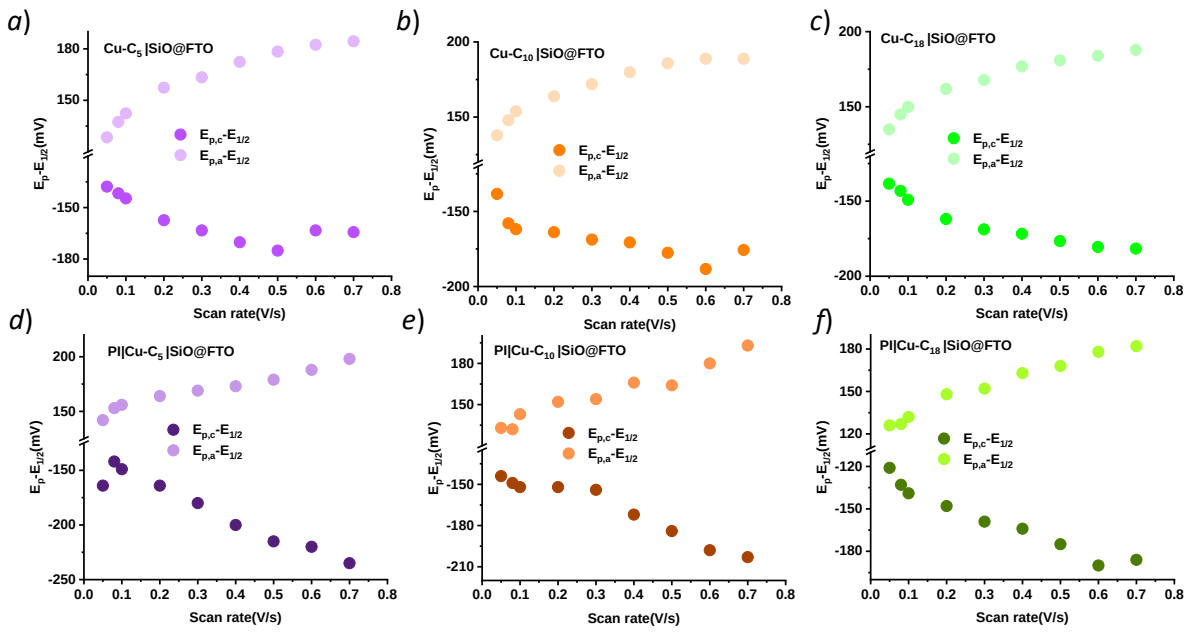

Figure S15. Trumpet plot for Cu-R|SiO@FTO and PI|Cu-R|SiO@FTO (S = 1 cm^2, pH = 12.00, 0.1 M NaOH/NaOAc).

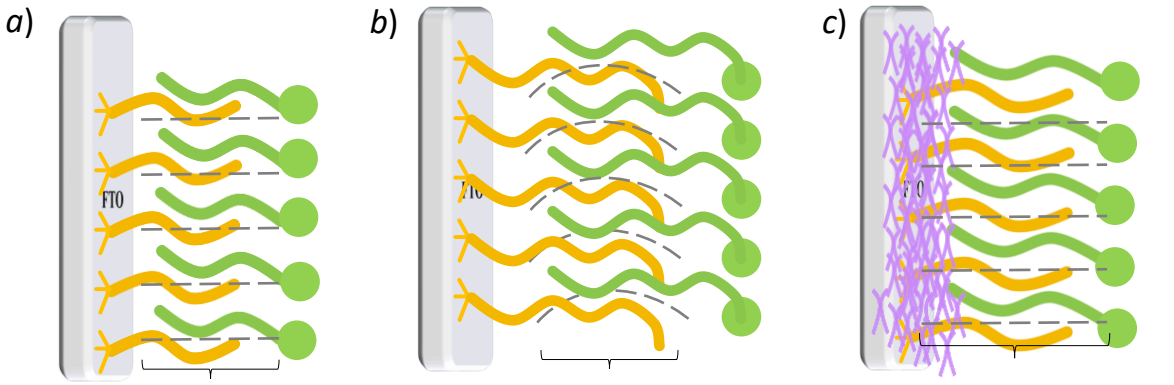

Scheme S4. Proposed SABs with different length of alkyl chain before and after encapsulation.

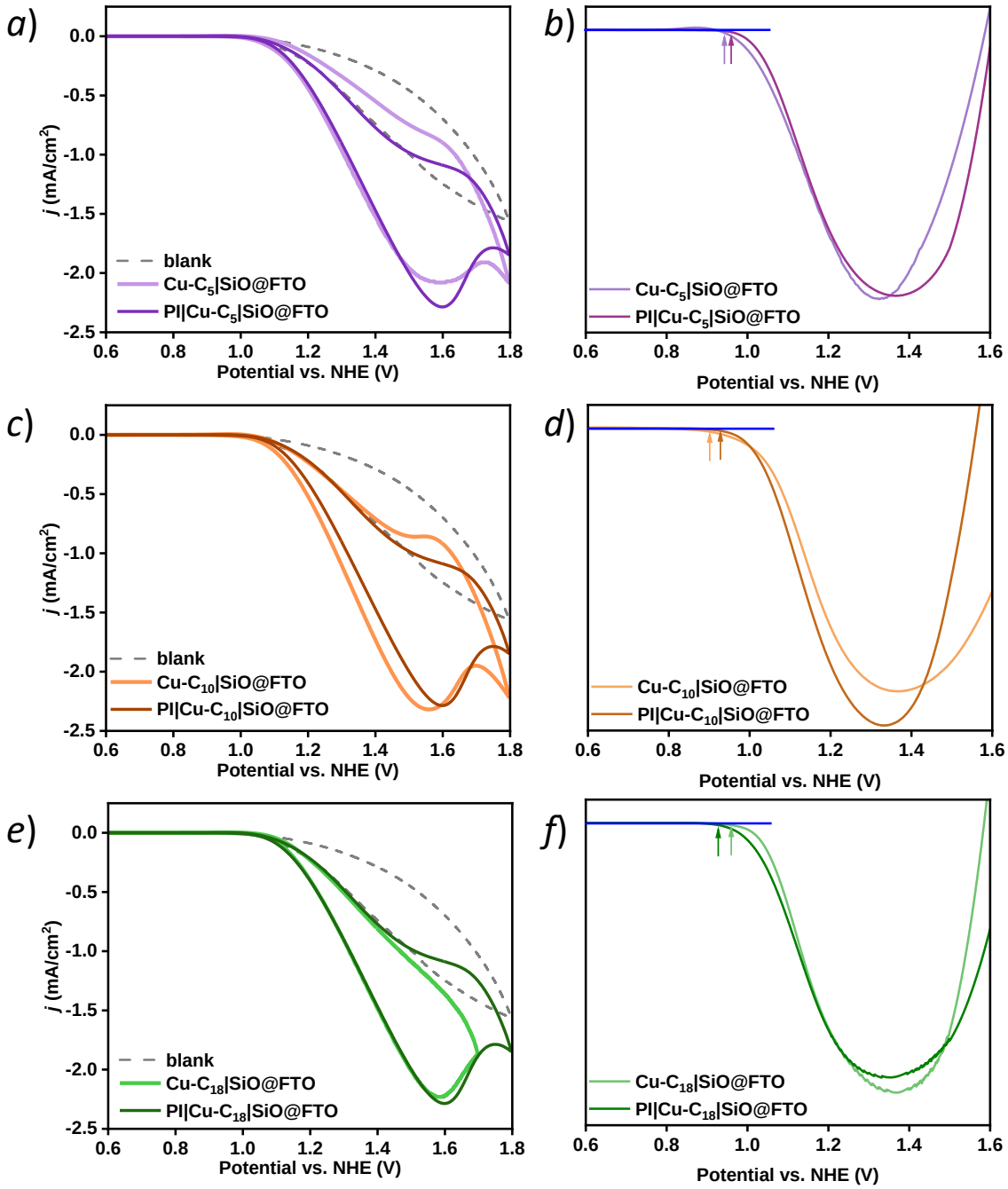

Figure S16. (left) CVs of Cu-R|Si@FTO and Pl|Cu-R|Si@FTO for water oxidation (S = 1 cm^2, pH = 12.00, 0.1 M NaOH/NaOAc, blank = bare FTO). (right) The numerical derivative of the first half data between 0.6 V ~ 1.6 V. Arrows indicate the inflection point, i.e. onset potentials.

The TOF value is calculated from the equation S4:

$$TOF = \frac{J \times A}{n \times F \times \Gamma} \qquad \text{(eq. S4)}$$

where J is the current density at 1.6 V, A is the surface area of the electrode (1 cm^2), n is the transferred electrons, F is the Faraday constant, and Γ is the surface coverage.

Table S3. Comparison of electrochemical behavior of Cu-R|Si@FTO and PI|Cu-R|Si@FTO at pH 12 buffer solution.

Sample	Γ^a (nmol/cm^2)	$E_{ox}(Cu^{II/I})$ (V_{NHE})	$E_{re}(Cu^{II/I})$ (V_{NHE})	Peak-to-peak separation ($Cu^{II/I}$) (V_{NHE})	$E_{1/2}$ (V_{NHE})	η^b (V_{NHE})	$E_{WO}{}^c$ (V_{NHE})
$Cu(pimH)(OH_2)_2$[d]	/	0.250	-0.275	0.525	-0.0125	0.85	1.50
Cu-C_5|SiO@FTO	0.1350	0.228	-0.059	0.287	0.085	0.94	1.57
PI|Cu-C_5|SiO@FTO	0.0301	0.188	-0.149	0.337	0.020	0.96	1.59
Cu-C_{10}|SiO@FTO	0.0738	0.239	-0.054	0.293	0.093	0.94	1.61
PI|Cu-C_{10}|SiO@FTO	0.0182	0.177	-0.118	0.295	0.030	0.96	1.55
Cu-C_{18}|SiO@FTO	0.0941	0.241	-0.057	0.298	0.093	0.96	1.58
PI|Cu-C_{18}|SiO@FTO	0.0173	0.151	-0.120	0.271	0.016	0.93	1.59

The above cyclic voltammetry tests were performed at pH 12.00 buffer of 0.1M NaOH/NaOAc with a scan rate of 100mV/s.

[a]Γ were calculated according to ref[10].

[b]Onset potentials of the catalysts according to ref[11].

[c]Water oxidation potentials.

[d]Data were collected from ref[5].

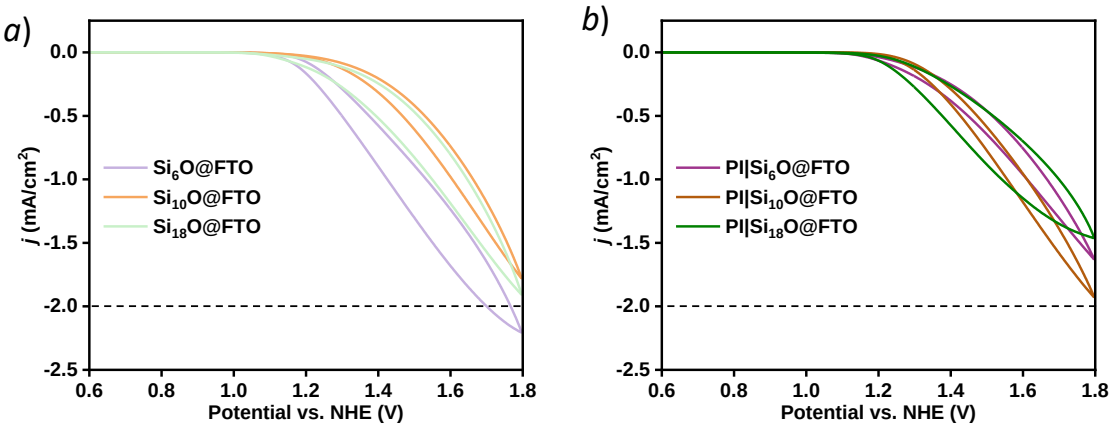

Figure S17. CVs of a) SiO@ FTO and b) CVs of PI|SiO@FTO for water oxidation (S = 1 cm^2, pH = 12.00, 0.1 M NaOH/NaOAc). As we expected, these monolayered aliphatic chains passivate the FTO electrodes and decrease the oxidative current of the bare FTO.

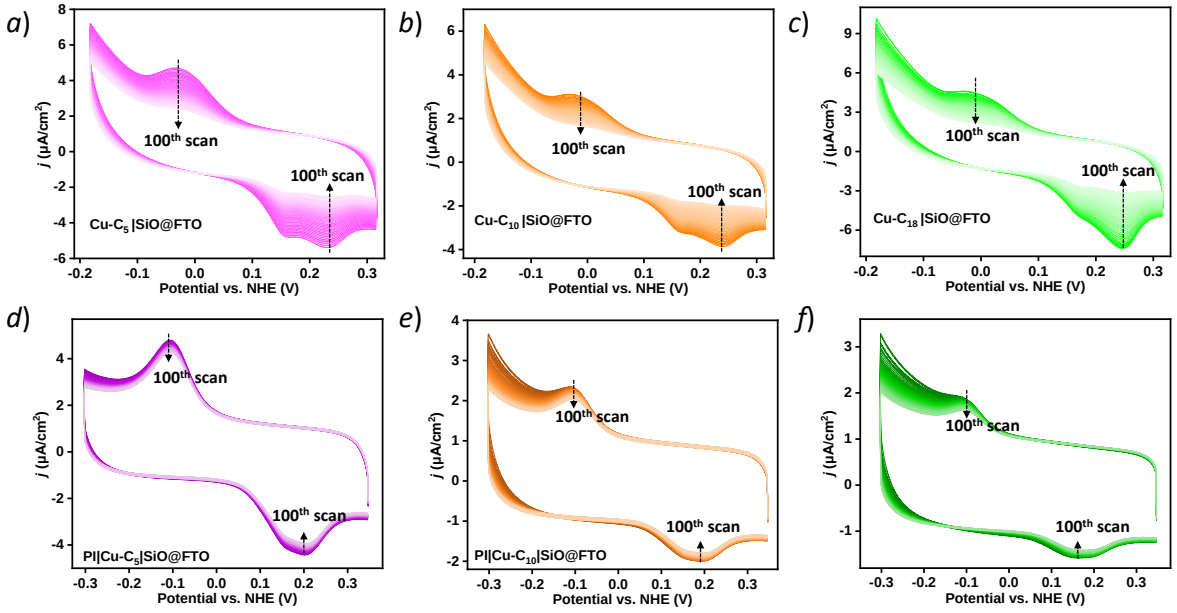

Figure S18. Consecutive cyclic voltammetry cycles for (a) Cu-C_5|SiO@FTO, (b) Cu-C_{10}|SiO@FTO, (c) Cu-C_{18}|SiO@FTO, (d) PI|Cu-C_5|SiO@FTO, (e) PI|Cu-C_{10}|SiO@FTO and (f) PI|Cu-C_{18}|SiO@FTO with a scan rate of 100 mV/s at the pH = 12 of 0.1 M NaOAc/NaOH buffer solution under N_2 atmosphere.

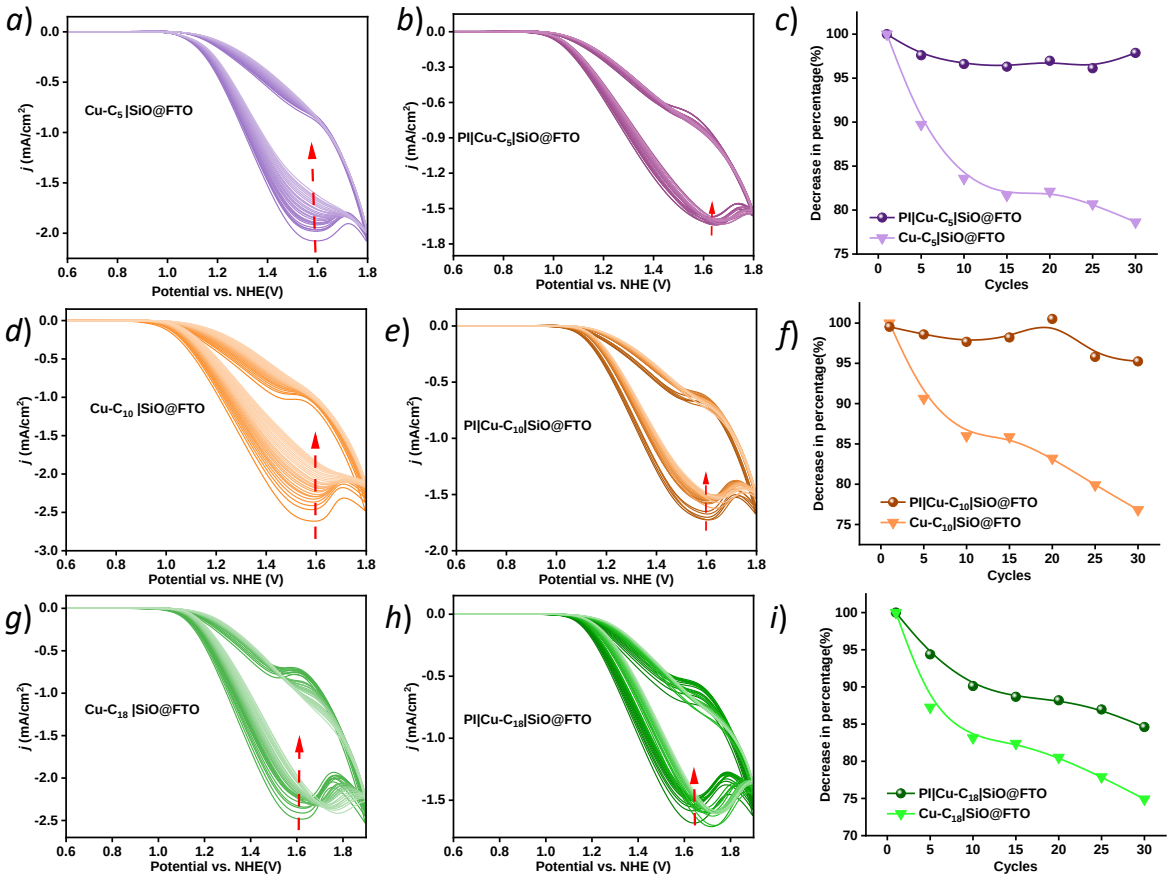

Figure S19. CVs of (a, d, g) Cu-R|SiO@FTO and (b, e, h) CVs of PI|Cu-R|SiO@FTO (Number of sweep cycles:30, sweep speed: 100 $mV \cdot s^{-1}$). (c, f, i) Peak current changes versus sweep cycles.

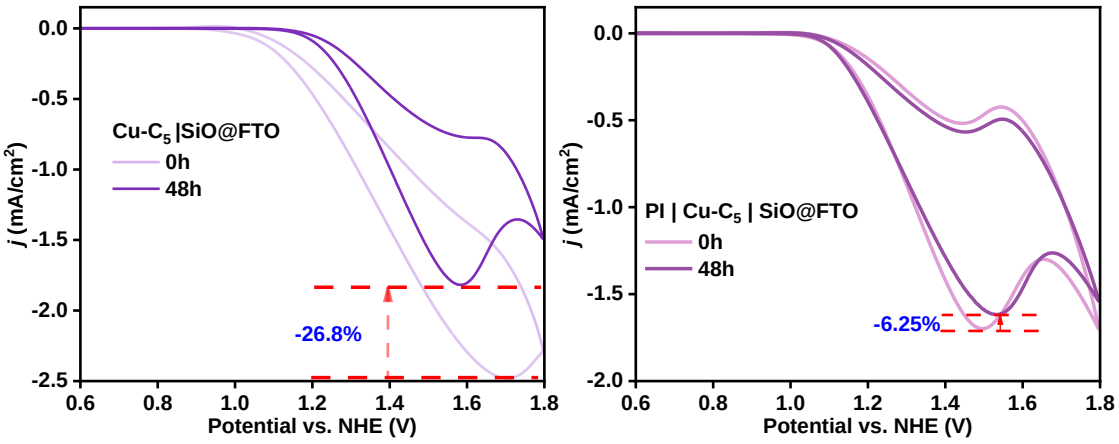

Figure S20. CVs of Cu-C_5|SiO@FTO and PI|Cu-C_5|SiO@FTO before and after immersing in pH 12 NaOAc/NaOH buffer solution for 48 h.

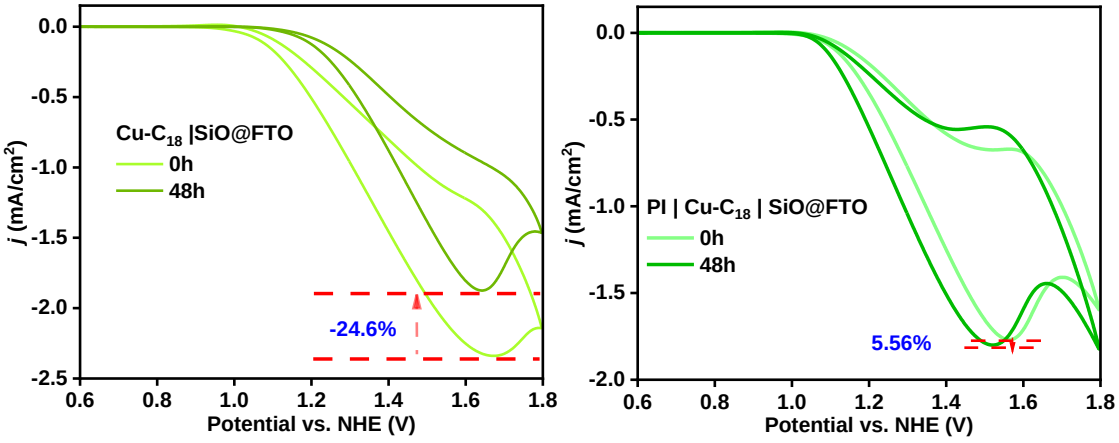

Figure S21. CVs of Cu-C_{18}|SiO@FTO and PI|Cu-C_{18}|SiO@FTO before and after immersing in pH 12 NaOAc/NaOH buffer solution for 48 h.

Faradaic efficiency (FE) calculations

The collector−generator electrode setup is done by a previously reported method[12]. Fabrication of a collector−generator assembly began with cutting 10 mm by 40 mm pieces of FTO. The upper right corner of each cell was removed with a diagonal cut from upper left to approximately 8−10 mm down from the top along the right lateral edge. Then 3M electrical tape were bonded to the upper left corner of the electrodes. Thin (3 mm wide) pieces of 1 mm thick microscope slides were epoxied (3M Marine Adhesive Sealant) along the lower lateral edges of the conductive face of the FTO collector electrode. Using the same inert epoxy, the generator electrode (with catalysts on surface) was then bonded to the collector with the conductive sides facing. For the generator-collector configuration, the bipotentiostat poised the working generator electrode at a set potential (1.65 V vs NHE) while the collector (FTO) electrode was poised at -0.65 V vs NHE for in-situ reduction of the generated O_2. Prior to electrocatalysis, the buffer solution was degassed with Ar for 30 min. The currents were normalized to the geometric areas of the working electrodes. The currents were normalized to the geometric areas of the working electrodes. Then the Faradaic efficiency was calculated according to equation S5.

$$FE = \frac{Q_{Col} - Q_{background}}{Q_{Gen} \times \eta} \qquad \text{(eq. S5)}$$

where $Q_{Col} - Q_{background}$ is the integrated charge passed at the FTO collector electrode with reducing the background charge, Q_{Gen} is the integrated charge at the generator electrode. Here, we take η = 70% as the recognized collection efficiency for the cell according to previous studies[12, 13].

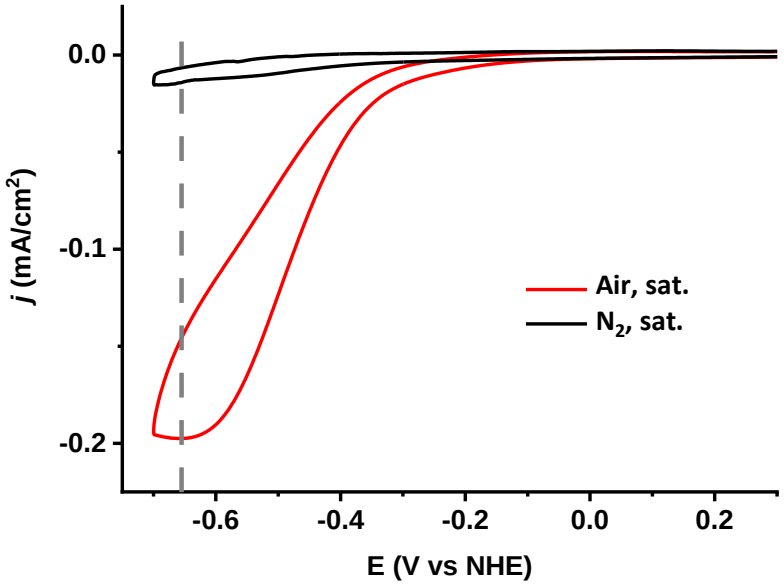

Figure S22. Cyclic voltammograms taken at a planar FTO electrode in 0.1 M NaOAc/NaOH buffer at pH 12 saturated with air (red), or N_2 (black), confirming the potential of collector at -0.65 V vs NHE is suitable.

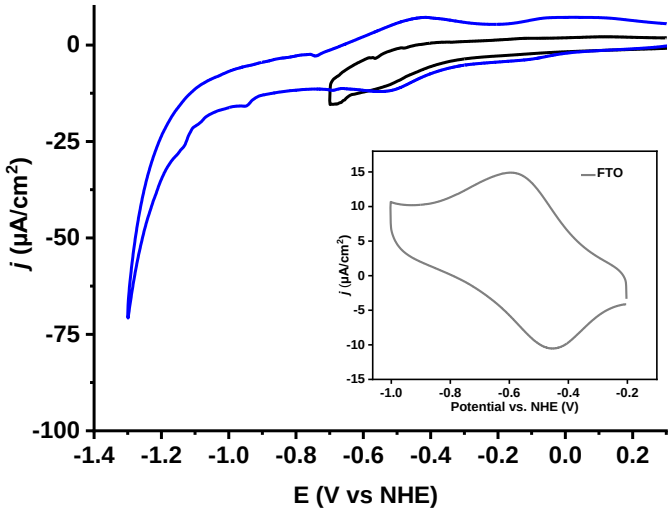

Figure S23. Cyclic voltammograms taken at a planar FTO electrode in N_2 saturated solution showing the onset of hydrogen formation at potentials more negative than −0.9 V vs NHE. Inset: CV of planar FTO in N_2 degassed 0.1 M NaOH/NaOAc buffer at pH ~ 12.00.

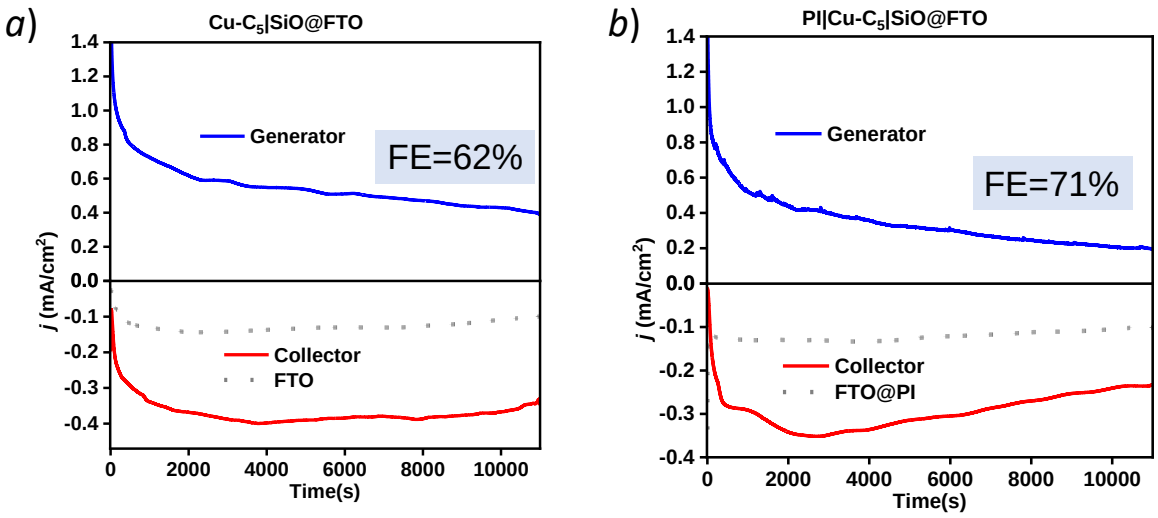

Figure S24. Current-time traces of Cu-C_5|SiO@FTO and PI|Cu-C_5|SiO@FTO over 3 hours at a FTO generator electrode at 1.65 V (vs. NHE) for catalytic water oxidation (solid blue line), and cathodic current-time traces at the FTO collector electrode at −0.65 V (vs. NHE) for simultaneous O_2 detection (solid red line), relative to a FTO working electrode as the control sample to eliminate background current and small leaks in the N_2 atmosphere (dotted gray line). The electrolysis using the generator-collector configuration was carried out at pH ~ 12.00 in a 0.1 M NaOH/NaOAc buffer under N_2 atmosphere. The currents were normalized to the geometric areas of the electrodes.

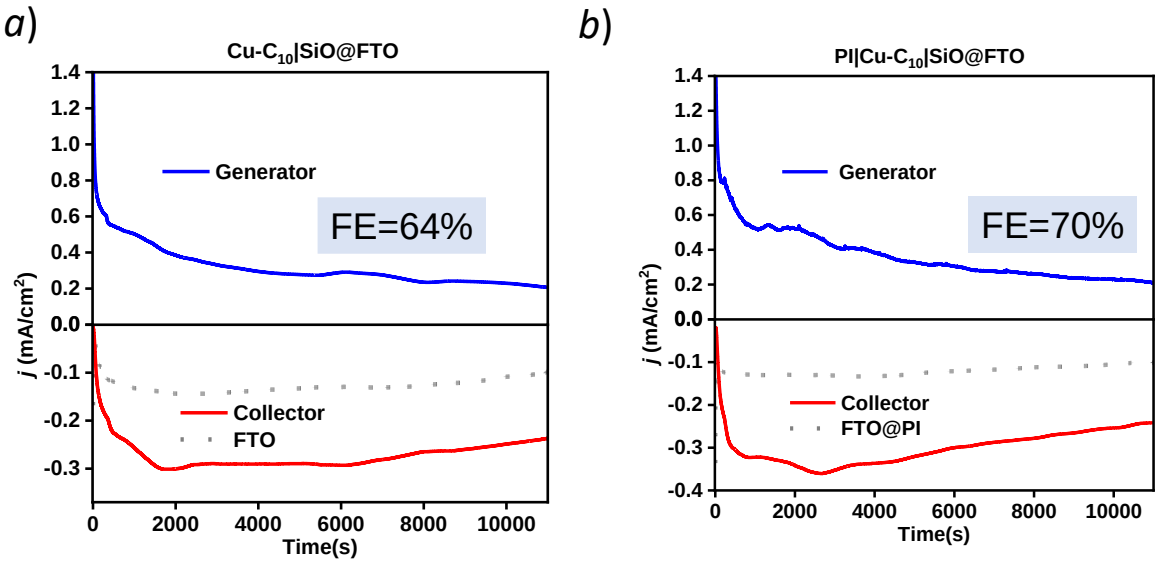

Figure S25. Current-time traces of Cu-C_{10}|SiO@FTO and PI|Cu-C_{10}|SiO@FTO over 3 hours at a FTO generator electrode at 1.65 V (vs. NHE) for catalytic water oxidation (solid blue line), and cathodic current-time traces at the FTO collector electrode at −0.65 V (vs. NHE) for simultaneous O_2 detection (solid red line), relative to a FTO working electrode as the control sample to eliminate background current and small leaks in the N_2 atmosphere (dotted gray line). The electrolysis using the generator-collector configuration was carried out at pH ~ 12.00 in a 0.1 M NaOH/NaOAc buffer under N_2 atmosphere. The currents were normalized to the geometric areas of the electrodes.

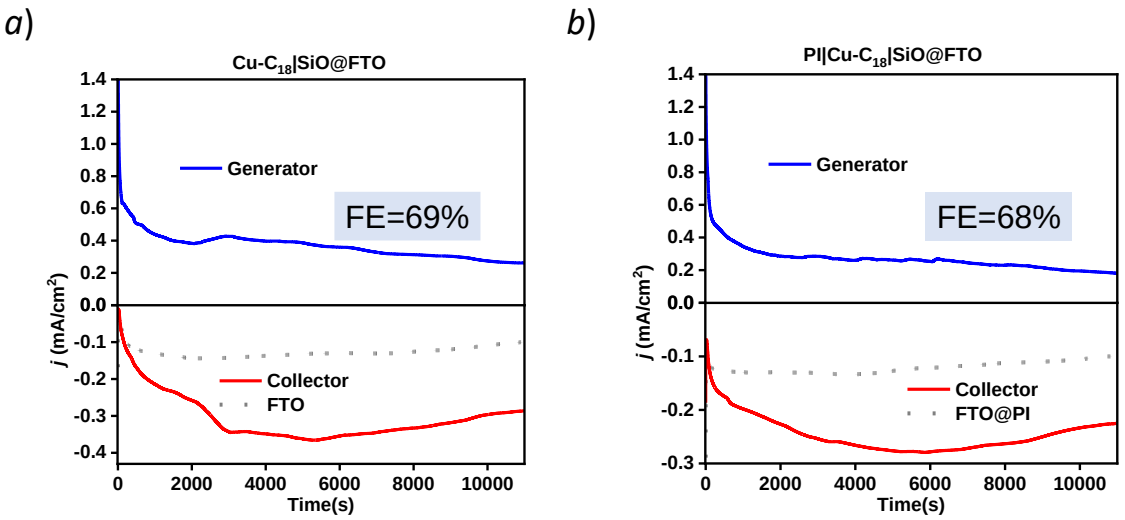

Figure S26. Current-time traces of Cu-C_{18}|SiO@FTO and PI|Cu-C_{18}|SiO@FTO over 3 hours at a FTO generator electrode at 1.65 V (vs. NHE) for catalytic water oxidation (solid blue line), and cathodic current-time traces at the FTO collector electrode at −0.65 V (vs. NHE) for simultaneous O_2 detection (solid red line), relative to a FTO working electrode as the control sample to eliminate background current and small leaks in the N_2 atmosphere (dotted gray line). The electrolysis using the generator-collector configuration was carried out at pH ~ 12.00 in a 0.1 M NaOH/NaOAc buffer under N_2 atmosphere. The currents were normalized to the geometric areas of the electrodes.

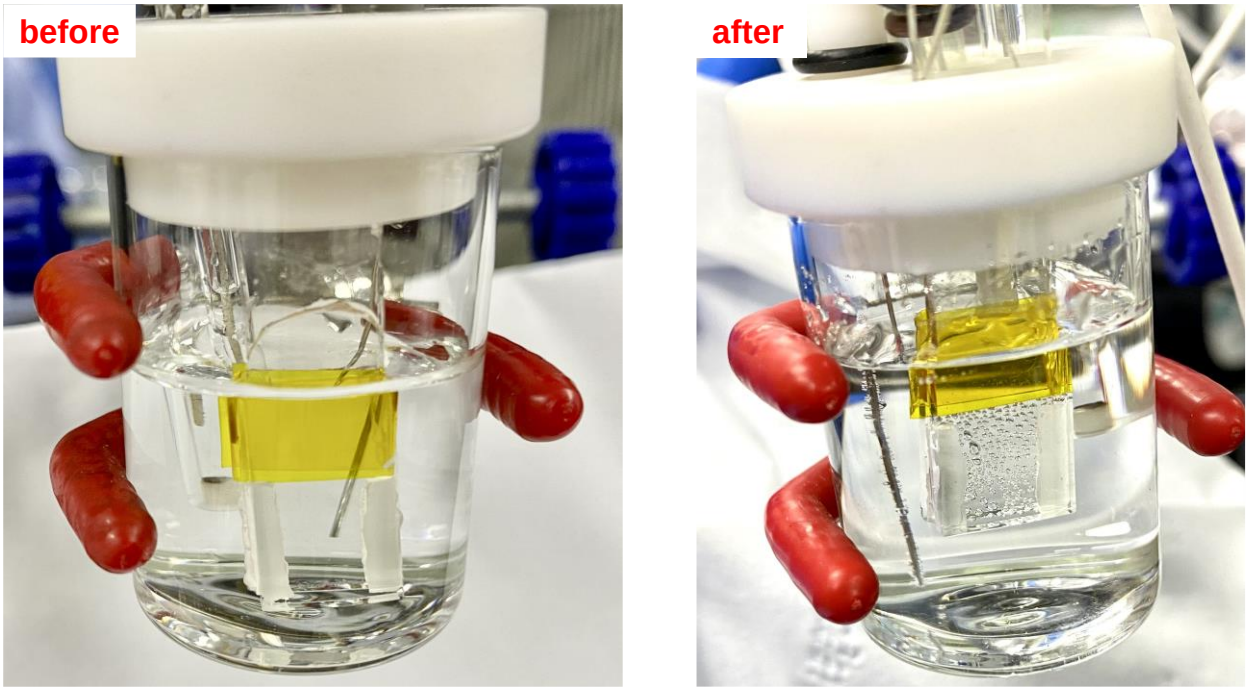

Figure S27. G-C setups for FE measurement. Bubbles are observed during FE measurement.

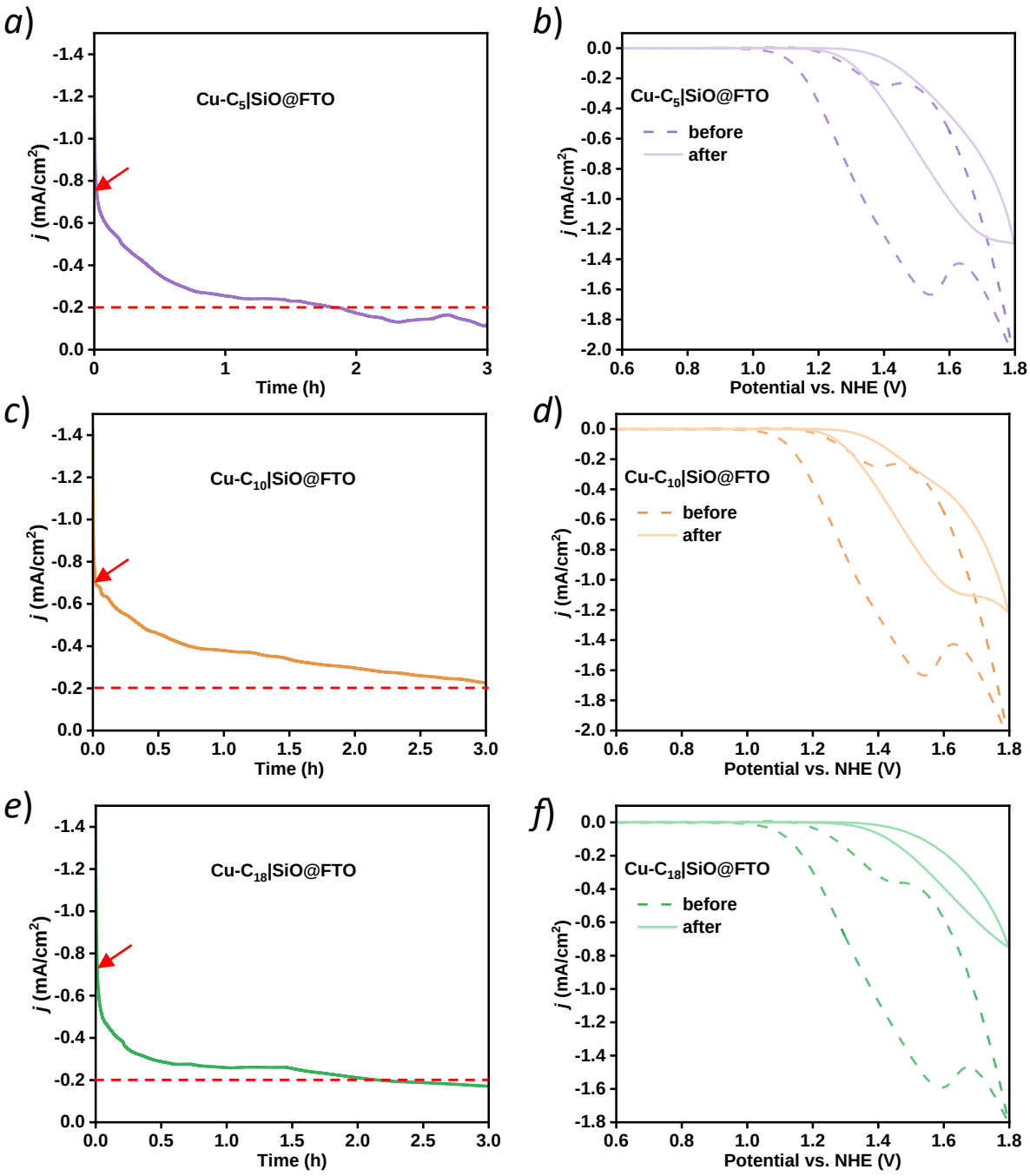

Figure S28. (left) Current density of a representative CPE experiment for Cu-R|SiO@FTO over 3 hours at the potential of 1.65 V vs NHE. Condition: pH ~ 12.00 in a 0.1 M NaOH/NaOAc buffer. (right) CVs for Cu-R|SiO@FTO before and after CPE.

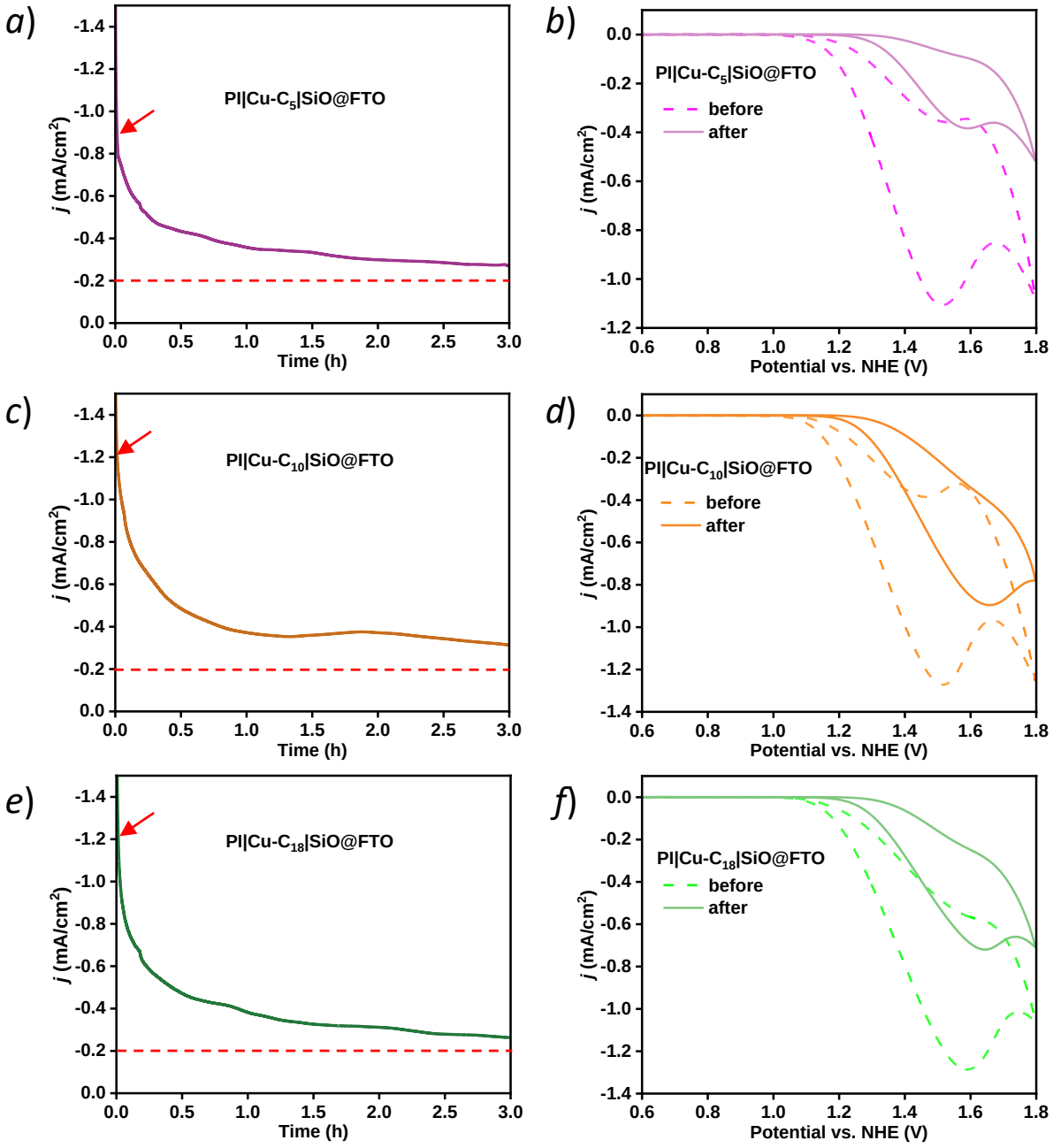

Figure S29. (left) Current density of a representative CPE experiment for PI|Cu-R|SiO@FTO over 3 hours at the potential of 1.65 V vs NHE. Condition: pH ~ 12.00 in a 0.1 M NaOH/NaOAc buffer. (right) CVs for PI|Cu-R|SiO@FTO before and after CPE.

After 3 hours of CPE, the CV showed that the water oxidation peak almost disappeared when compared with the protected PI|Cu-R|SiO@FTO samples showing obvious water oxidation behaviors. The obvious difference strongly supports the positive **"protection"** effect of PI on surfaces**.**

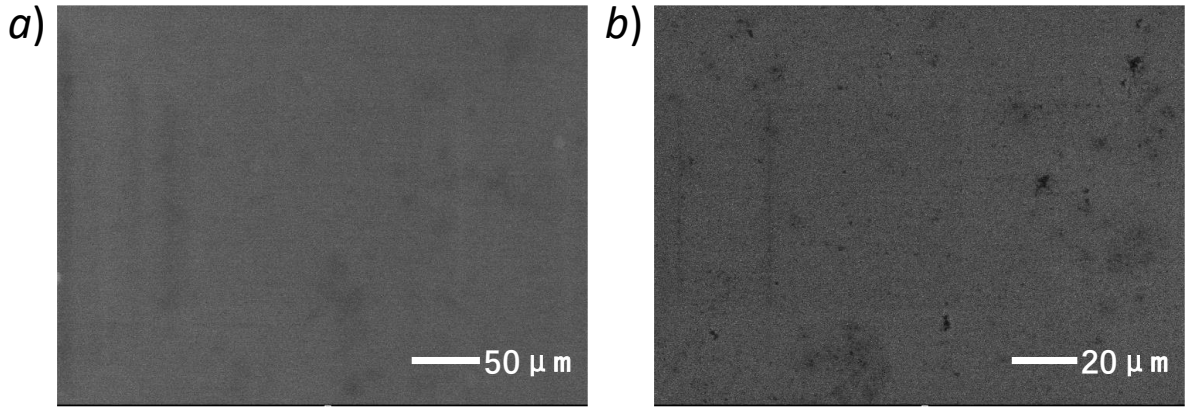

Figure S30. SEM image of PI|Cu-R|SiO@FTO after I-t experiment. The morphology doesn't show obvious change after electrolysis compared to Figure S7.

Table S4. Comparison of water oxidation performance of Cu-R|Si@FTO and PI|Cu-R|Si@FTO. Condition: pH ~ 12.00 in a 0.1 M NaOH/NaOAc buffer.

Sample	α^b	$k_s{}^b$	TOF (s^{-1})	FE (%)
$Cu(pimH)(OH_2)_2{}^a$	/	/	35	/
Cu-C_5|SiO@FTO	0.834	0.309	36 ± 2.5	62 ± 4.5
PI|Cu-C5|SiO@FTO	0.322	0.195	198 ± 14.8	71 ± 12.7
Cu-C_{10}|SiO@FTO	0.593	0.169	56 ± 11.5	64 ± 6.0
PI|Cu-C10|SiO@FTO	0.413	0.210	312 ± 17.5	70 ± 6.6
Cu-C_{18}|SiO@FTO	0.568	0.171	44 ± 2.1	69 ± 9.0
PI|Cu-C_{18}|SiO@FTO	0.463	0.219	359 ± 10.6	68 ± 11.7

[a]Data from ref[5].

[b]α and k_s are calculated at a scan rate of 200 mV/s.

Examples of polymerization strategies for stabilizing molecular complexes

For example, Meyer and co-workers attached the vinyl-derivatized water oxidation catalyst $[Ru(Mebimpy)(dvbpy)(OH_2)]^{2+}$ on the electrode by surface electropolymerization[13]. Badiei and co-workers prepared plasma-grafted poly(acrylic acid) (PAA) on the FTO surface (PAA|FTO) and immobilized $[Ru\text{-}OH_2]^{2+}$-type water oxidation catalysts on the PAA|FTO by using the hydrogen-bond interaction between ligated water molecule and carboxylate groups on PAA[14, 15]. Ott and co-workers incorporated $[Ru(tpy)(dcbpy)(OH_2)]^{2+}$ water oxidation catalysts into UiO-67-grown FTO thin films by post-synthetic ligand exchange[16].

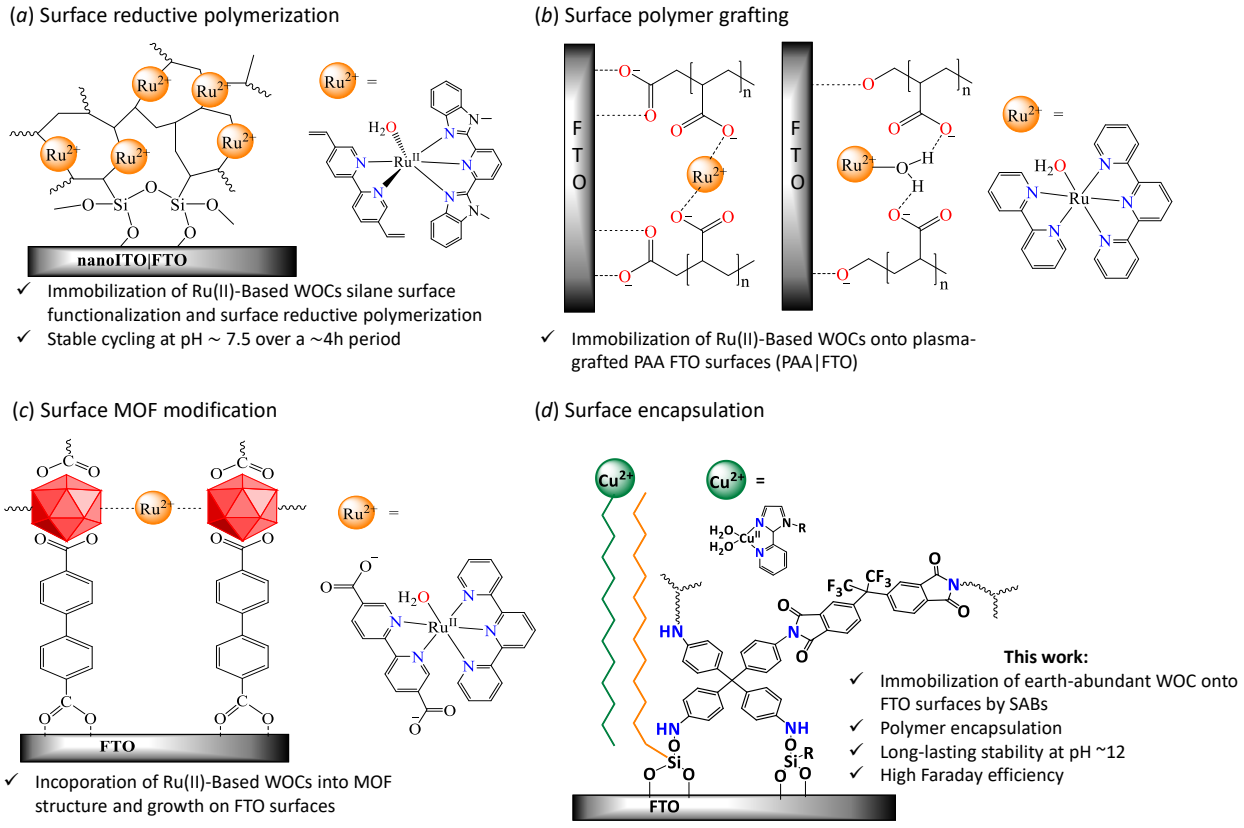

Scheme S5. Examples of polymerization strategies for stabilizing molecular complexes.

Table S5. Examples of heterogenization strategies for immobilizing copper molecular catalysts.

Catalyst	Heterogenization Strategy	Buffer pH[c]	Stability	Catalyst Performanc[d]	Ref
$[Cu(pimR)(OH)_2]$	SAB + Surface Polymerization	0.1 M ABS (pH 12.0)	0.9 mA/cm^2 @1.65V ~1h 0.5 mA/cm^2 @1.65V ~4h	TOF ~359 s^{-1}	This work
$[Cu(TMC)(H_2O)](NO_3)_2]$[a]	Nafion-CC	0.1 M PBS (pH 7)	1mA/cm^2 @1.64V ~4h	TOF ~30 s^{-1}	Ref [17]
$[Cu(TEOA)(H_2O)_2][SO_4]$	Electrodeposition on ITO	0.1 M ABS (pH 12.4)	0.55 mA /cm^2 @1.30V ~3h	Tafel slope~ 130 mV/dec	Ref[18]
$[Cu^{II}(en)_2(OH_2)_2]^{2+}$	Electrodeposition on $Cu(OH)_2$/CuO nanoparticles@ ITO	0.2 M PBS (pH 12.0)	2.5 mA /cm^2 @1.15V ~6 h	Tafel slope~ 62 mV/dec	Ref[19]
$[Cu^{II}$(TPA) $H_2O](ClO_4)_2$[b]	Electrodeposition on CuO nanoparticles@ ITO	0.2 M BBS (pH 9.2)	1.4 mA /cm^2 @1.41V ~2h	Tafel slope~ 56 mV/dec	Ref[20]

[a] TMC = 1,4,8,11-tetramethyl 1,4,8,11 tetraazacyclotetradecane
[b] TPA = tris(2-pyridylmethyl)amine
[c] ABS: acetate buffer solution; PBS: phosphate buffer solution; BBS: borate buffer solution
[d] Best condition in the report

References

1. R. Wang, J.-C. Xiao, B. Twamley, M. S. J. O. Jean'ne and B. Chemistry, 2007, **5**, 671-678.
2. A. Juris, V. Balzani, F. Barigelletti, S. Campagna, P. Belser and A. von Zelewsky, *Coord. Chem. Rev.*, 1988, **84**, 85-277.
3. S. M. Barnett, K. I. Goldberg and J. M. Mayer, *Nat. Chem.*, 2012, **4**, 498-502.
4. R. Wang, J.-C. Xiao, B. Twamley and M. S. Jean'ne, *Org. Biomol. Chem.*, 2007, **5**, 671-678.
5. L. A. Stott, K. E. Prosser, E. K. Berdichevsky, C. J. Walsby and J. J. Warren, *ChemComm*, 2017, **53**, 651-654.
6. L. Wang, D. E. Polyansky and J. J. Concepcion, *J. Am. Chem. Soc*, 2019, **141**, 8020-8024.
7. T. Zhang, C. Wang, S. Liu, J.-L. Wang and W. Lin, *J. Am. Chem. Soc.*, 2014, **136**, 273-281.
8. M.-T. Zhang, Z. Chen, P. Kang and T. J. Meyer, *J. Am. Chem. Soc.*, 2013, **135**, 2048-2051.
9. K. J. Fisher, K. L. Materna, B. Q. Mercado, R. H. Crabtree and G. W. Brudvig, *ACS Catal.*, 2017, **7**, 3384-3387.
10. D. L. Ashford, B. D. Sherman, R. A. Binstead, J. L. Templeton and T. J. Meyer, *Angew. Chem. Int. Ed.*, 2015, **54**, 4778-4781.
11. C. Batchelor-McAuley, *Current Opinion in Electrochemistry*, 2022, 101176.
12. B. D. Sherman, M. V. Sheridan, C. J. Dares and T. J. Meyer, *Anal. Chem.*, 2016, **88**, 7076-7082.
13. L. Wu, A. Nayak, J. Shao and T. J. Meyer, *Proc. Natl. Acad. Sci. U.S.A.*, 2019, **116**, 11153-11158.
14. Y. M. Badiei, O. Annon, C. Maldonado, E. Delgado, C. Nguyen, C. Rivera, C. Li and A. F. Ortega, *ChemElectroChem*, 2023, **10**, e202300028.
15. Y. M. Badiei, C. Traba, R. Rosales, A. L. Rojas, C. Amaya, M. Shahid, C. Vera-Rolong and J. J. Concepcion, *ACS Appl. Mater. Interfaces*, 2021, **13**, 14077-14090.
16. B. A. Johnson, A. Bhunia and S. Ott, *Dalton Trans.*, 2017, **46**, 1382-1388.
17. F. Yu, F. Li, J. Hu, L. Bai, Y. Zhu and L. Sun, *ChemComm*, 2016, **52**, 10377-10380.
18. T.-T. Li, S. Cao, C. Yang, Y. Chen, X.-J. Lv and W.-F. Fu, *Inorg. Chem.*, 2015, **54**, 3061-3067.
19. C. Lu, J. Du, X.-J. Su, M.-T. Zhang, X. Xu, T. J. Meyer and Z. Chen, *ACS Catal.*, 2016, **6**, 77-83.
20. X. Liu, H. Jia, Z. Sun, H. Chen, P. Xu and P. Du, *Electrochem Commun*, 2014, **46**, 1-4.